Memoirs of the School of Engineering, Okayama University Vol. 20, No. 2, February 1986

SAXS from the GP Zones in Al-4mass%Cu Alloy at Initial Stages of Ageing

Masuo Yamada*, Mutsuo Ohta* and Akira Sakakibara*

(Received February 19, 1986)

Synopsis

A series of small-angle X-ray scattering photographs with monochromated and point focussed copper $K\alpha_1$ radiation was taken of a single crystal of an Al-4mass%Cu alloy at the as-quenched state from 823K and at successive stages of ageing at 313K. The crystal was so oriented that the incident direction of the radiation was along [001] axis, and was cooled with liquid nitrogen during the exposure.

The pattern of the as-quenched state was homogeneous, but each of the patterns of the aged states consisted of streaks along [100] and [010] directions and a quasi-ring around the trace of the incident beam on the film (even at the shortest ageing time, 16sec). The most intense regions were found in [100], [010], [100] and [010] directions on the ring. With the progress of the ageing the streaks and the ring became more intense and narrower.

The results can be interpreted from points of view of the formation of the GP zones parallel to {100} planes ab initio, the effect of the inter-particle interference on scattering of X-rays, and the growth of the GP zones with the ageing. Guinier radius of the GP zones at each stage can be obtained from intensity change along [110], and the values are reasonably consistent with those obtained from the cross section of the streak. The presence of multi-layer zones, besides the one-layer ones, is suggested from the humps found on several intensity curves along [100] at later stages.

* Department of Industrial Science

INTRODUCTION

GP zones have been widely studied[3]-[5], since they were found in Al-Cu alloys by Guinier[1] and Preston[2] as clusters of solute atoms coherent to the matrix. X-ray methods have been frequently adopted in these studies to investigate structures of GP zones and precipites and their relation to age-hardening process of the alloy. Structures of GP zones were revealed mainly by means of measurement of intensity of X-ray diffuse scattering besides recent lattice-image method of TEM.[6]-[8] Auvray et al.[9] studied the alloy aged for 12 years at room temperature and reported the existence of GP zones consisting of two or more atomic layers. Silcock et al,[10] Graf[11] and Kawano et al.[12] determined average diameter of GP zones from SAXS intensity ditribution of the streak measured in its cross-section. Although there are not many reports on the scattering in the extreme vicinity of the origin of reciprocal space, as Naudon et al.[13],[14] pointed out, Toman[15] found, using CuKα radiation, remarkable increase in intensity in the region below 2° of scattering angle, but Gerold[16] denied the result.

Naudon et al,[13] by means of CuKα radiation and PSPC, measured variation of SAXS intensity along [100] and [110] during ageing at 293K and found maximum in intensity around 2°, though the values of intensity were very different in the two directions. They considered the maximum to be due to spinodal decomposition of the alloy. Rioja and Laughlin[17] studied electron diffraction from the alloy aged for more than 5hr at room temperature and found satellite spots near the reciprocal lattice points. They interpreted it to be due to modulation of solute concentration caused by spinodal decomposition.

In the measurement of anisotropic SAXS intensity such as in the case of Al-Cu alloy, point-focussing collimation and two-dimensional observation are indispensible to survey the whole aspect of the scattering. It is also necessary to depress background intensity for studying initial ageing process. In this paper, results obtained from photographic measurements of the SAXS intensity using a point-focussing monochromater are reported.

2. EXPERIMENTAL PROCEDURES

Plates of single crystal, 0.5 mm thick and 5 mm wide, were made from Al-4mass%Cu Alloy(nominal composition) by strain-annealing

method. A plate, whose plane normal was near [100], was chosen by transmission Laue method. The plate was chemical-polished in 10%NaOH aqueous solution at about 340K and electro-polished in perchloric acid-ethanol (1:4) solution to the thickness of about 0.15 mm. To avoid deformation during quenching and handling, specimen was spot-welded to a window-shaped holder of pure aluminium. The specimen, after solution treatment at 823K for 1hr, was quenched into iced water, transfered quickly into the liquid nitrogen bath, and then ageing at 313K and SAXS measurement were repeated by turns. SAXS intensity was measured in the same way as previously reported,[18],[19] and the direction of incidence was [001] of the specimen.

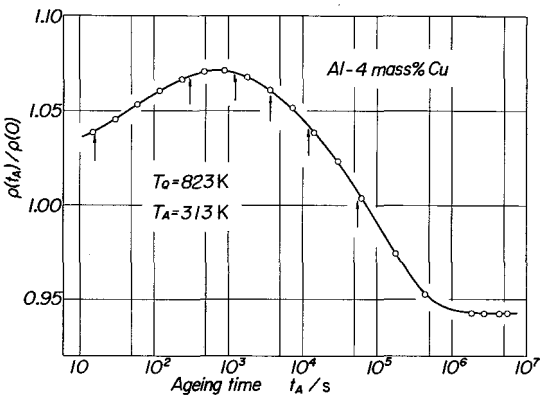

Fig.1 Fractional resistivity change of polycrystalline Al-4mass%Cu alloy quenched from 823K on ageing at 313K.

In this study small change in intensity distribution scattered from the specimen at the as-quenched and the initial ageing stage needed to be detected. In order to confirm the reliability of the photographic measurement, SAXS from the same specimen was measured both by the photographic method and by a counter method. The specimen used for this purpose was Al-15mass %Zn polycrystalline quenched from 623K and aged at 313K for 30hr. Spherical GP zones were expected to form by this heat treatment. Because of the saturation of blackening of the film, several photographs were taken with various exposure times and the intensity curves were jointed together to obtain the whole profile by superposing the curves in the region where D was between 0.1 and 0.2. In the counter method, RIGAKU SAXS apparatus was used with an NaI(Tl) scintillation detecter and a PHA adjusted to CuKα radiation. More than 1000 counts were accumulated at each angle.

Resistivity of a polycrystalline specimen made of the same Al-4mass%Cu alloy as was used in SAXS experiment was measured during ageing after the same heat treatment. In Fig.1 the resistivity change is shown and the stages at which SAXS measurement was made are indicated by arrows.

3. RESULTS

3.1 Comparison between methods of intensity measurement

Fig.2 shows intensity curves obtained by different measurements. Measurements by photograph (O) and by the counter (□) are compared at first using incidence filtered by an Ni foil of 20μm thick. In the high angle region beyond 0.3 nm^{-1} of s (=2sinθ/λ, 2θ:scattering angle, λ:wavelength), intensity profiles are found to be very different. On the other hand, the curve obtained by the counter using incidence monochromated by an LiF crystal agrees well with the curve obtained by the photographic method. Therefore, the accuracy of the measurement by the two methods, photographic and by the counter, can be considered to be almost the same. Abnormal intensity which appeared when Ni filter and counter were used together was caused by fluorescence from Zn atoms in the specimen excited by the short wavelength component in the incidence which passed through the Ni filter. Marks ▼ and ▲ in the figure are the SAXS intensities obtained by placing another filter,

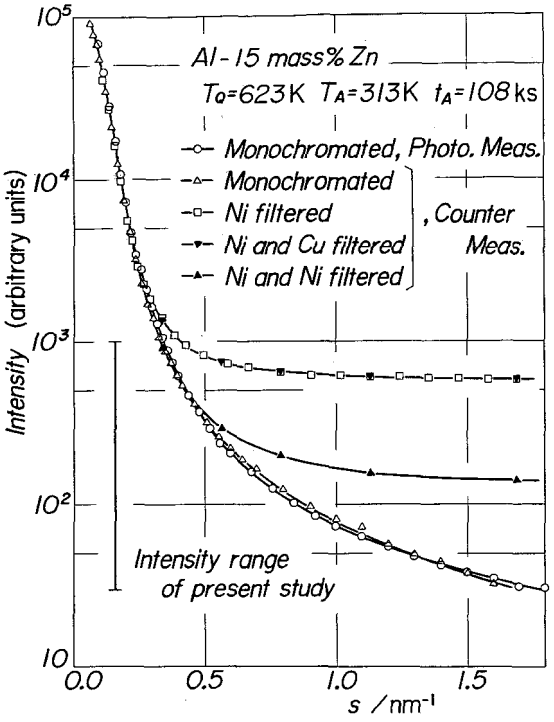

Fig.2 Comparison between the present photographic measurement (O) and counter measurements. In the counter measurements, the beam was monochromated (△) or filtered with Ni foil (□), and in addition to the filter for the incident beam, the scattered radiation was again filtered with Cu foil (▼) or Ni foil (▲) just in front of the counter.

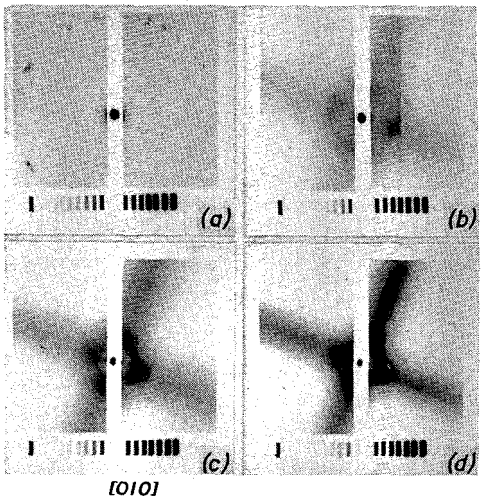

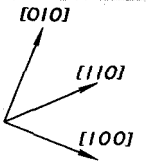

Photo 1 Scattering patterns at as-quenched state (a) and at aged ones. Ageing times at 313K are 16s(b), 0.3ks(c) and 1.2ks(d).

Cu and Ni respectively, in front of the counter. X-ray tube was operated at 40 kV always in this experiment. In the case of Al-4mass% Cu alloy, fluorescence from Cu atoms in the specimen must be expected and therefore monochromatization is essential in this study.

Range of the SAXS intensity from the Al-Cu alloy was relatively narrow, D being between 0.03 and 1.0 in all photographs (between 300 and 1000 for the value in Fig.2).

3.2 SAXS intensity measurement

Photo 1 shows the photographs taken at the as-quenched and the initial ageing stages. In each film, a spot at the centre is the trace of the incident beam, a long and narrow unexposed part around the spot is the shadow of the Cu beam stopper, and the distance from

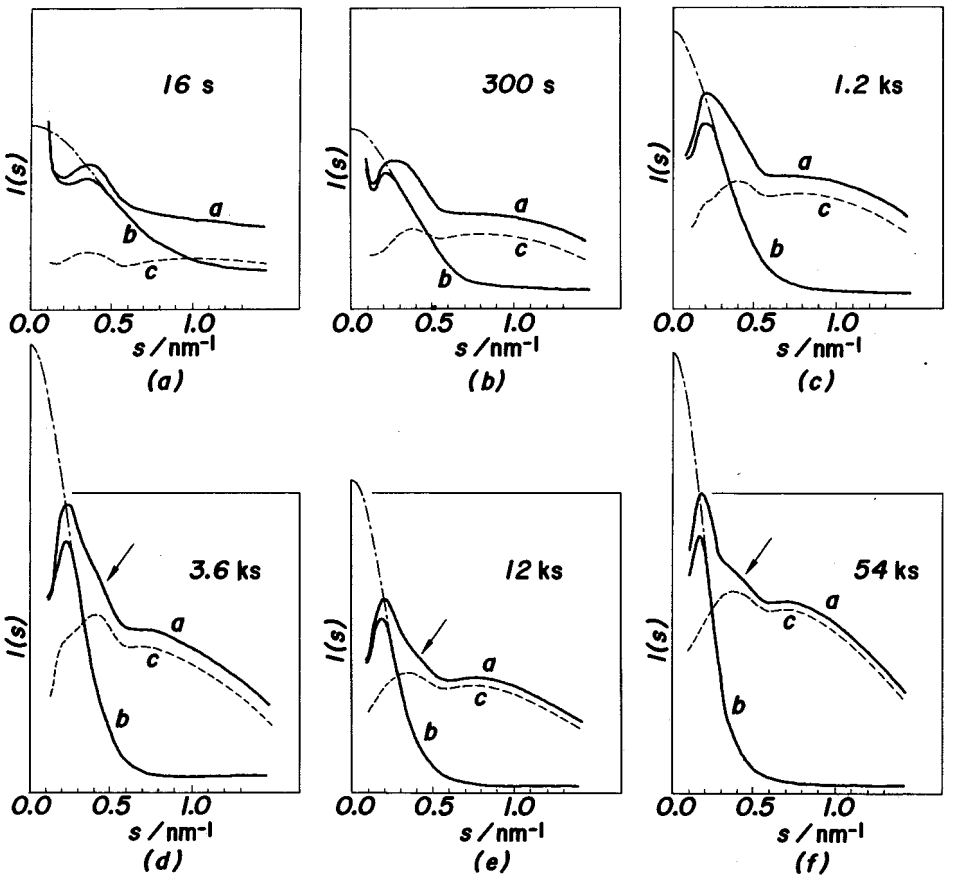

Fig.3 Scattered intensities along [100], a, and [110], b, at several stages of ageing at 313K. A chained line in each figure is extrapolation by Guinier approximation and a broken line, c, which will be explained in text, is streak intensity calculated from curves a and b.

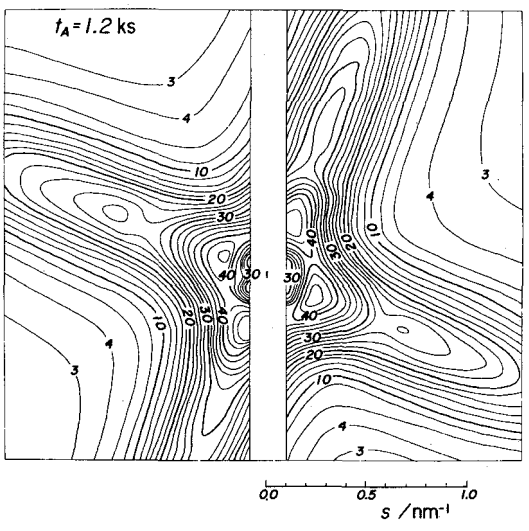

Fig.4 Equi-intensity contour map of the photograph at the ageing time of 1.2ks. A vertical rod at the centre is a trace of the direct beam.

the incident spot to the film edge corresponds to about 1.5 nm^{-1} of s. Intensity distribution at the as-quenched state is uniform, which indicates that GP zones are not yet formed. After ageing for 16s, however, intensity distribution changes, and weak and rather wide streaks can be observed along [100] and [010] direction. This reveals ready clustering of solute atoms to form plate-like GP zones at this stage. Moreover, ring-shaped distribution of intensity is recognized distinctly around the incident spot. Intensity profiles of the ring along the [100] and [110] direction are shown in Fig.3 with solid lines a and b, respectively. Intensity peaks reported also by Naudon et al.[13] in the intensity profile along these directions correspond to those in the curves. As is seen in photo 1 and Fig.3 SAXS pattern becomes more distinct and the ring radius smaller when the ageing proceeds, and even after ageing for 54ks existence of the ring is still recognized. Fig.4 shows an equi-intensity contour map of the film (40x35 mm^2) obtained from specimen aged for 1.2ks. Microphotometry was made along 35 transverse lines on the film. This figure reveals the following: Interval between contour lines is narrow near the centre, and hence intensity increases rapidly with s in this region. After passing through the maximum, intensity decreases greatly in the [110] and [1$\bar{1}$0] direction but it decreases at first greatly and then gradually in the [100] and [010] direction. Region where there occurs rapid change in intensity is seen as a ring in Photo 1. Intensity along the ring is maximum in the <100> directions. The contour map obtained by Naudon et al.[14] is similar to that in Fig.4.

4. DISCUSSION

Intensity distribution and its evolution during ageing, shown in

Photo 1, Fig.3 and Fig.4, can be understood by considering that plate-like GP zones were formed readily at the initial stage of ageing and grown with ageing. This view may be sound because of the early appearance of streaks in the <100> directions at the stage of 16s ageing. Phillips[6] also recognized plate-like zones in the specimen which was not thought to proceed much with decomposition after solution treatment by means of high-resolution, high-magnification TEM observation. Therefore, in the following, distribution of SAXS intensity obtained will be discussed, not from the standpoint of Rioja and Laughlin[17], but from the standpoint that there have been already formed plate-like zones from the early stage of ageing.

Consider 3N GP zones in the irradiated volume V of the specimen, planes of N zones being parallel to (100), (010) and (001) each. Scattering intensity of all zones can be written as

$$I(\vec{s})=\sum_{g}^{3N}\sum_{h}^{3N} F_g(\vec{s})F_h(\vec{s})\cos(2\pi\vec{s}\cdot\vec{R}_{gh}) \qquad (1)$$

in electron unit. $F_g(\vec{s})$ and $F_h(\vec{s})$ are the structure factor of the g-th and h-th GP zone, centre of which are $|\vec{R}_{gh}|$ apart. Strictly speaking, lattice deformation around a zone plate and therefore its contribution to the structure factor must be allowed for. But Kawano et al.[12] showed that diffuse scattering caused by this lattice deformation could be neglected near the origin of the reciprocal lattice, because of the small difference in electron density relative to the core plane of Cu atoms. Denoting average structure factor of GP zones parallel to (100), (010) and (001) by $\overline{F_x(\vec{s})}$, $\overline{F_y(\vec{s})}$, and $\overline{F_z(\vec{s})}$ respectively and assuming that zones in each plane are the same in their structure, we obtain

$$\begin{aligned}I(\vec{s})=N\{&\overline{F_x(\vec{s})}^2+\overline{F_y(\vec{s})}^2+\overline{F_z(\vec{s})}^2\}+\overline{F_x(\vec{s})}^2\sum_i\sum_{j\neq i}\cos(2\pi\vec{s}\cdot\vec{R}_{ij})\\&+\overline{F_y(\vec{s})}^2\sum_k\sum_{l\neq k}\cos(2\pi\vec{s}\cdot\vec{R}_{kl})+\overline{F_z(\vec{s})}^2\sum_m\sum_{n\neq m}\cos(2\pi\vec{s}\cdot\vec{R}_{mn})\\&+2\overline{F_x(\vec{s})}\,\overline{F_y(\vec{s})}\sum_i\sum_k\cos(2\pi\vec{s}\cdot\vec{R}_{ik})+2\overline{F_y(\vec{s})}\,\overline{F_z(\vec{s})}\sum_k\sum_m\cos(2\pi\vec{s}\cdot\vec{R}_{km})\\&+2\overline{F_z(\vec{s})}\,\overline{F_x(\vec{s})}\sum_m\sum_i\cos(2\pi\vec{s}\cdot\vec{R}_{mi})\end{aligned}$$

where subscripts (i,j), (k,l) and (m,n) designate zones parallel to (100), (010) and (001) planes respectively.

Let us denote by $P_{xx}(\vec{r})$, $P_{xy}(\vec{r})$ and $P_{xz}(\vec{r})$ the distribution function of the centre of the second zone parallel to (100), (010) and (001) respectively when the centre of the first zone parallel to (100) is at the origin. $P_{yx}(\vec{r})$, ..., $P_{zz}(\vec{r})$ represent similarly. Generally, relations $P_{xy}(\vec{r})=P_{yx}(\vec{r})$, $P_{yz}(\vec{r})=P_{zy}(\vec{r})$ and $P_{zx}(\vec{r})=P_{xz}(\vec{r})$ hold and six functions are then independent. Now, we assume that

spacial distribution of zones does not depend on their orientation and hence is isotropic, i.e., $P_{xx}(\vec{r})=\ldots=P_{zz}(\vec{r})=P(r)$.

considering N>>1, all double sums in Eq.(2) give [20),(21)

$$\sum\sum\cos(2\pi\vec{s}\cdot\vec{R})=\frac{N^2}{V}\int_V P(\vec{r})\cos(2\pi\vec{s}\cdot\vec{r})dv=\frac{N^2}{V}\int_0^\infty P(r)\frac{\sin(2\pi sr)}{2\pi sr}4\pi r^2dr$$
$$=N\frac{\rho}{3}\int_0^\infty P(r)\frac{\sin(2\pi sr)}{2\pi sr}4\pi r^2dr \qquad (3)$$

where ρ is the zone density. Eq.(3) is denoted by Np(s). Function p(s) represents interference effect between scattering waves and has the same content in practically observable region as the reverse sign of inter-particle interference function given by Gerold[22]. This function p(s) is nearly equal to N at s=0, and decreases drastically with s at first. As s increases further, p(s) becomes less than 1 in most cases, depending on the distribution function P(r). Value of p(s) then decreases gradually with s and finally approaches to 0 near around $s\sim 1/r_0$, r_0 being the distance at which P(r) approaches to 1. Substituting this function in Eq.(2) gives

$$I(\vec{s})=N\{\overline{F_x(\vec{s})}^2+\overline{F_y(\vec{s})}^2+\overline{F_z(\vec{s})}^2\}\cdot\{1+p(s)\}$$
$$+2Np(s)\{\overline{F_x(\vec{s})}\,\overline{F_y(\vec{s})}+\overline{F_y(\vec{s})}\,\overline{F_z(\vec{s})}+\overline{F_z(\vec{s})}\,\overline{F_x(\vec{s})}\} \qquad (4)$$

Consider zones as circular disks, R in radius and 2t(<<R) in thickness. Square of the average inertial distance with respect to the incidence parallel to [001] of the crystal are $(R\sin\phi)^2/4+(t\cos\phi)^2/3$, $(R\cos\phi)^2/4+(t\sin\phi)^2/3$ and $R^2/4$ respectively for the zones parallel to (100), (010) and (001), hence by Guinier approximation are given

$$\overline{F_x(\vec{s})}^2=\overline{F_x(s,\phi)}^2=F(0)^2\exp\{-4\pi^2s^2(\frac{R^2}{4}\sin^2\phi+\frac{t^2}{3}\cos^2\phi)\} \qquad (5a)$$
$$\overline{F_y(\vec{s})}^2=\overline{F_y(s,\phi)}^2=F(0)^2\exp\{-4\pi^2s^2(\frac{R^2}{4}\cos^2\phi+\frac{t^2}{3}\sin^2\phi)\} \qquad (5b)$$
$$\overline{F_z(\vec{s})}^2=\overline{F_z(s,\phi)}^2=F(0)^2\exp(-4\pi^2s^2\frac{2R^2}{4}) \qquad (5c)$$

where ϕ is the angle from [100] to [010] in the (001) plane. Intensity distribution in the [100] direction is given approximately by substituting Eq.(5) with $\phi=0$ into Eq.(4)

$$I_{[100]}(s)=I_s(s)+I_{h1}(s) \qquad (6)$$

where

$$I_s(s)=NF(0)^2\exp(-4\pi^2s^2\frac{2t^2}{3})\cdot\{1+p(s)\} \qquad (6a)$$
$$I_{h1}(s)=2NF(0)^2\exp(-4\pi^2s^2\frac{2R^2}{4})\cdot\{1+4p(s)\exp(4\pi^2s^2\frac{2R^2}{16})\} \qquad (6b)$$

Intensity distribution in the [110] direction is given by Eq.(5) with $\phi=\pi/4$, approximately as

$$I_{[110]}(s)=3NF(0)^2\exp(-4\pi^2s^2\frac{2R^2}{6})\cdot\{1+3p(s)\}\equiv I_{h2}(s) \quad (7)$$

Difference between $3NF(0)^2\exp(-4\pi^2s^2R^2/6)$ and $\overline{F_x(s)}^2+\overline{F_y(s)}^2+\overline{F_z(s)}^2$, i.e., the difference between the curves d and e in Fig.5(a) is a few percent in the observable range of s.

If p(s) is known, scattering intensity can be calculated by Eqs. (6) and (7), but no report on the spacial distribution of GP zones are found at present. Inverse calculation of p(s) and then P(r) from experimentally obtained scattering intensity could be carried out, but it is practically difficult because size distribution of the zones is unknown and because intensity values at extremely small s cannot be measured.

Curves a-d in Fig.5(a) are the results calculated by Eqs.(6) and (7) when p(s)=0, R=1.0 nm and t=0.1 nm. Intensity curve along [100], $I_{[100]}(s)$ hardly changes in the region of large s and corresponds to the streak. It stems from $I_s(s)$. Experimental $I_{[100]}(s)$, however,

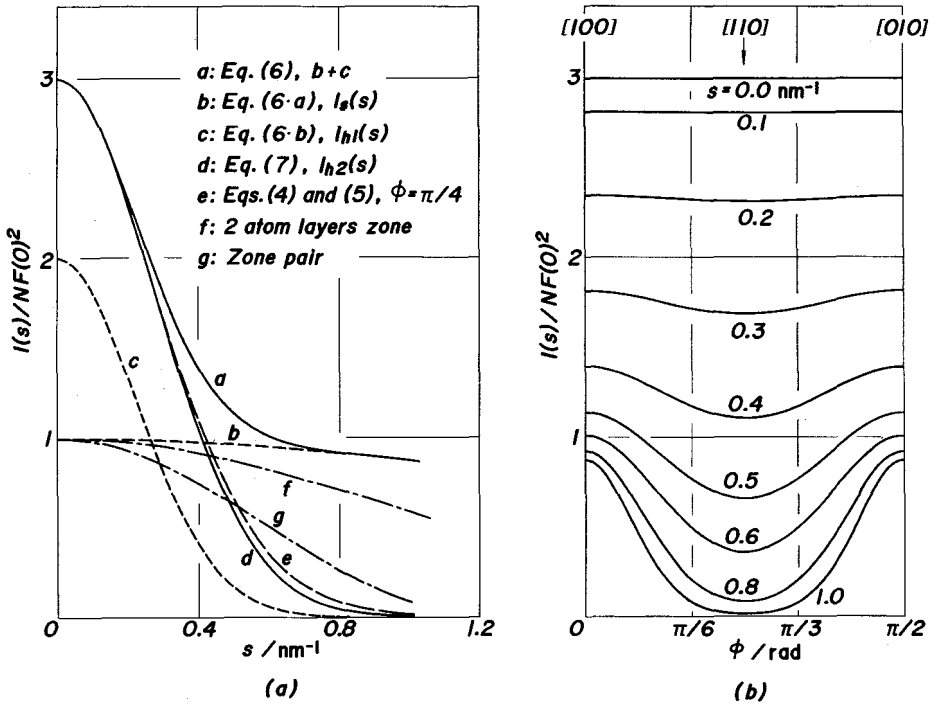

Fig.5 (a) Calculated intensities along [100],a, b, c, f and g; and along [110], d and e. Curves a, b, c, d and e are calculated assuming R=1.0 nm and t=0.1 nm. Curve b represents [100] streak. Curves f and g are respective intensities of two-atom-layer zones and of zone-pair, both normalized at $s=0\ nm^{-1}$ to 1. (b) Angular dependence of intensities calculated from Eqs.(4) and (5) for several values of s, assuming p(s)=0.

changes considerably in the region, as is seen in Figs.3 and 4. This may be due partly to increasing departure of the Ewald sphere from

the centre line of the streak with increasing s.

At smaller s where p(s) is finite, $I_{h1}(s)$ and $I_{h2}(s)$ changes with s under its influence, but they decrease exponentially at larger s where p(s) is nearly equal to zero. They become large in relatively small s region and this region corresponds to the ring in the scattering pattern. Values of s where $p(s) \sim 0$ is considered to fall near the position where the curve b and the chained curve in each figure of Fig.3 coincide. Chained curves represent exprapolation of respective curves b with Guinier approximation and hence correspond to the case where p(s)=0. This value of s decreases with the progress of ageing, which means that r_0 value where $P(r) \sim 1$ increases, i.e., mean distance between nearest zones increases, with ageing. It may be considered that difference between the curve b and the chained curve in the small s region is caused by the difference of p(s) from zero.

Fig.5(b) shows angular(ϕ) variation of intensity from [100] to [010] calculated from Eqs.(5) and (4) for several values of s, neglecting inter-particle interference, i.e., assuming p(s)=0. For a certain value, intensity takes maximum in the <100> direction and minimum in the <110> direction. In the present model, p(s) is assumed to have spherical symmetry, and then similar angular variation may be expected for the case $p(s) \simeq 0$. Experimental result described in Chapter 3 that intensity variation along the ring takes the maximum value in the <100> direction can be thus understood qualitatively.

Guinier radius, R_G^h, corresponding to the average radius of zone disks is obtained using Eq.(7) from the intensity variation along [110] and is shown in Table 1 (2nd column). In the 3rd column of the table are shown Guinier radius R_G^s obtained as usual from the streak.

Table 1 Guinier radii obtained from intensities along [110], R_G^h and from streak, R_G^s.

t_A/ks	R_G^h/nm	R_G^s/nm
0.3	0.86	1.07
1.2	1.03	1.19
3.6	1.17	1.25
12	1.38	1.49
54	1.54	1.67

In order to obtain R_G^s, intensity distribution in the transverse cross-section of the streak at a certain s value ($0.6\ nm^{-1} < s < 0.8\ nm^{-1}$) determined for each photograph is measured under the condition that other intensity than that of streak is weak, i.e., intensity of the ring in its tail is weak. Values of R_G^h and R_G^s generally agree well, but R_G^h is relatively small and the difference is rather larger at shorter ageing times. This difference may be due to the difference in conditions of obtaining respective values, as follows: Intensity distribution used to obtain R_G^s is in the transverse cross-section at

relatively large s value in the [100] direction where influence of the halo ring is small. In this case deviation of the Ewald sphere from the centre line of the streak (about 0.05 nm^{-1}) has little effect on the result as far as the reflection rod has axial symmetry, because slope of plots, log(I) vs. s^2, is used. On the other hand, intensity distribution used to calculate R_G^h is the part of $I_{[110]}(s)$ for relatively small s values; therefore, influence of inter-particle interference and that of small zones must be allowed for.

A hump is observed between 0.3 and 0.6 nm^{-1} of s in the intensity curve along [100] for the specimen aged for 5.4ks (indicated by an arrow in Fig.3(f)a). This tendency is seen also from 3.6ks ageing. Comparing Eqs.(6) and (7), it is found that

$$I_{[100]}(s)-(2/3)\cdot\{I(0)\}^{-1/2}\cdot\{I_{[110]}(s)\}^{3/2} \qquad (8)$$

gives values of Eq.(6a), i.e., the streak intensity $I_s(s)$ for small p(s). Dashed curve c in each figure of Fig.3 represents this intensity. Curve c, different form curve b in Fig.5(a) calculated for one-layer zones, has a maximum in the s region where the hump is observed in curve a. This maximum appears from the biginning of ageing. Positions of the maximum observed are 0.37, 0.39, 0.41, 0.41, 0.35, 0.38 nm^{-1} for Fig.3(a)-(f), respectively.

Function p(s) in Eq.(6a) was at first defined as a inter-particle interference function of zones parallel to (100) plane, i.e., transformation of $P_{xx}(r)$, although next, from Eq.(2) to Eq.(4), discussion was made on the assumption that $P_{xx}(r)\ldots$ are all equal to P(r). Therefore, the fact that Eq.(8) and hence the curve c in Fig.3 has small values in the small s region may be due to interference between scattering waves from those zones. When interference evaluated from the curve b of Fig.3 is applied to the curve b of Fig.5(a), intensity decreases in the small s region, but this alone does not explain the behaviour of the curve c of Fig.3 enough. Since intensity of the curve c of Fig.3 in the large s region ($s>0.6$ nm^{-1}) corresponds to that of the curve b of Fig.5(a), it is sound to consider that other scattering intensity must be added in the region around the maximum of the curve c of Fig.3. Judging from the behaviour around the maximum, this additional intensity must decrease rapidly with s.

Auvray et al.[9] reported detailed analysis of the X-ray diffuse scattering on this alloy aged at room temperature. They concluded that there were multi-layer zones besides one-layer zones of Cu atoms in the state of so-called GP(I) zones. Phillips[6], using bright field image and lattice image of TEM, also observed one-layer zones,

two-layer zones and "zone pairs". Recently Sato et al.[8] showed multi-layer zones by lattice image observation of TEM. These multi-layer zones are considered to present more rapid decrease in scattering intensity with s than the one-layer ones in the direction of the plane normal of the zone disk. The behaviour expected is shown in the curves f and g in Fig.5(a). Profile of the curve c in Fig.3 can be explained qualitatively by considering together the largely s-dependent scattering from multi-layer zones, scattering from one-layer zones and interference effect at small s. Therefore, other complex zones than one-layer ones are believed to be formed from the beginning of ageing, but their volume fraction may be small as estimated from the behaviour of curve c in Fig.3.

In Fig.3, the maximum of the curve c lies at larger value of s than the maximum of the curves a and b. This suggests that the assumption for the distribution function of zones to be isotropic is invalid at least between the zones whose planes are parallel each other and that they distribute more closely in the plane normal direction. Miyazaki et al.[23], evaluating the configurational stability of two plate-like γ' precipitates in Ni-Al alloy, showed that one of the most stable configurations is that they lie in the [100] direction and their planes are parallel each other. This suggests an similar effect for plate-like zones in Al-Cu alloy, but details are not yet understood.

ACKNOWLEDGEMENT

Thanks are giving to Mr. Toshiaki Kondo (graduate student, at present Komatsu Seisakusho Co. Ltd.) for cooperating in the measurement of SAXS intensity.

REFERENCES

(1) A. Guinier: Nature, 142(1938), 569.
(2) G. D. Preston: ibid., 570.
(3) H. K. Hardy and T. J. Heal: Progress in Metal Physics, Pergamon Press, 5(1954), 143.
(4) A. Kelly and R. B. Nicholson: Progress in Materials Science, Pergamon Press, 10(1963), 149.

(5) A. Guinier: Solid State Physics, Academic Press, 9(1959), 293.
(6) V. A. Phillips: Acta Met., 21(1973), 219.
(7) T. Takahashi, Y. Kojima, K. Mihama and Y. Ando: J. Japan Inst. Metals, 38(1974), 545.
(8) T. Sato, Y. Kojima and T. Takahashi: ibid., 45(1981), 803.
(9) X. Auvray, P. Georgopoulos and J. B. Cohen: Acta Met., 29(1981), 1061.
(10) J. M. Silcock, T. J. Heal and H. K. Hardy: J. Inst. Metals, 82(1953-54), 239.
(11) R. Graf: Publs. sci. et tech. ministère air, No.315(1956).
(12) O. Kawano, T. Hirouchi, H. Yoshida and Y. Murakami: J. Japan Inst. Metals, 35(1971), 1001.
(13) A. Naudon, J. Delafond, A. Junqua and J. Mimault: Scripta Met., 10(1976), 271.
(14) A. Naudon, J. Delafond, A. Junqua and J. Mimault: J. Appl. Cryst., 11(1978), 569.
(15) K. Toman: Acta Cryst., 10(1957), 187.
(16) V. Gerold: ibid., 11(1958), 230.
(17) R. J. Rioja and D. E. Laughlin: Met. Trans., 8A(1977), 1257.
(18) M. Ohta, M. Yamada, T. Kanadani, M. Hida and A. Sakakibara: J. Japan Inst. Metals, 42(1978), 946.
(19) M. Yamada and M. Ohta: Mem. Sch. Eng. Okayama Univ., 20(1985), 35.
(20) A. Guinier: Theorie et Technique de la Radiacristallographie, Dunod, Paris(1964).
(21) A. Guinier and G. Fournet: Small-Angle Scattering of X-rays, John Wiley & Sons, New York(1955).
(22) V. Gerold: Small-Angle X-ray Scattering, Proceedings of the Conference held at Syracuse University, 1965, Gordon and Breach, New York(1967), 277.
(23) T. Miyazaki, H. Imamura, H. Mori and T. Kozakai: J. Mater. Sci., 16(1981), 1197.